Chemical Science

ROYAL SOCIETY OF CHEMISTRY

EDGE ARTICLE

Cite this: *Chem. Sci.*, 2021, **12**, 13167

All publication charges for this article have been paid for by the Royal Society of Chemistry

"Concentration-in-Control" self-assembly concept at the liquid–solid interface challenged†

Gangamallaiah Velpula, *[a] Cristina Martin, [ab] Brent Daelemans, [a] Gunther Hennrich, [c] Mark Van der Auweraer, [a] Kunal S. Mali [a] and Steven De Feyter *[a]

Self-assembled molecular networks (SAMNs) on surfaces evoke a lot of interest, both from a fundamental as well as application point of view. When formed at the liquid–solid interface, precise control over different polymorphs can be achieved by simply adjusting the concentration of molecular building blocks in solution. Significant influence of solute concentration on self-assembly behavior has been observed, whether the self-assembly behavior is controlled by either van der Waals forces or hydrogen bonding interactions. In both cases, high- and low-density supramolecular networks have been observed at high and low solute concentrations, respectively. In contrast to this "concentration-in-control" self-assembly concept here we report an atypical concentration dependent self-assembly behavior at a solution–solid interface. At the interface between heptanoic acid (HA) and highly oriented pyrolytic graphite (HOPG), we show, using scanning tunneling microscopy (STM), the formation of a low-density porous network at high solute concentrations, and a high-density compact network at low solute concentrations. This intriguing inverse concentration dependent self-assembly behavior has been attributed to the preaggregation of solute molecules in the heptanoic acid solution as revealed by UV-vis spectroscopy. The observed results have been correlated to the molecular density of self-assembled monolayers attained at the HA/HOPG interface.

Received 31st May 2021
Accepted 6th September 2021

DOI: 10.1039/d1sc02950a

rsc.li/chemical-science

Introduction

Surface-confined molecular self-assembly of organic molecules is a popular approach to create patterned surfaces. In general, controlling the organization of building blocks into self-assembled molecular networks (SAMNs) at the liquid–solid interface is complex. Solute–solvent and solvent–substrate interactions have to be taken into the account in addition to the interactions between solute–solute and solute–substrate. Furthermore, external experimental conditions such as for example, temperature, pH, electric field and concentration are important parameters defining the outcome of the self-assembly process.[1–4]

Concentration dependent self-assembly has been well-explored in the past.[2,4–10] More than a decade ago, we have established the "concentration-in-control" self-assembly concept.[2] According to this concept, at high solute concentrations, molecules tend to form high density SAMNs, whereas the opposite is true at low solute concentrations, irrespective of the non-covalent interactions involved in the self-assembly process.[2,5] The tendency to form densely packed structures is due to lowering of the total free energy of the system taking into consideration the surface density of the adsorbed molecules. However, the formation of low-density supramolecular networks at low solution concentrations maximizes the energy gain of adsorbate–adsorbate and adsorbate–substrate interactions.[5,11]

This "concentration-in-control" self-assembly concept has been widely accepted until now for various building blocks, such as alkoxylated dehydrobenzo[12]annulene (DBA) derivatives,[2] alkoxylated benzene molecules,[8] different types of aromatic di-,[7] tri-,[6,10,12] and tetra-carboxylic acids[6] to name a few. The concentration dependent self-assembly of these derivatives at the liquid–solid interface has normally been investigated using scanning tunneling microscopy (STM).[6,7,10,12] Among the molecules that show SAMN formation, 3-fold symmetric tricarboxylic aromatic acids show a rich self-assembly behavior, including the formation of various structural polymorphs.[5,13–17] The relative abundance of these polymorphs depends on various parameters such as type of solvent,[15,18,19] temperature,[5,20] parameters that are imaging-related such as the electric field polarity between the STM tip and substrate, and importantly in the context of this study, the concentration.[12,21,22]

[a]*Division of Molecular Imaging and Photonics, Department of Chemistry, KU Leuven, Celestijnenlaan 200F, 3001 Leuven, Belgium. E-mail: gm.velpula@kuleuven.be; steven.defeyter@kuleuven.be*

[b]*Unidad NanoCRIB, Centro Regional de Investigaciones Biomédicas, Albacete-02071, Spain*

[c]*Universidad Autonoma de Madrid, Cantoblanco, 28049 Madrid, Spain*

† Electronic supplementary information (ESI) available. See DOI: 10.1039/d1sc02950a

For instance, benzene-1,3,5-tricarboxylic acid (trimesic acid – **TMA**) shows up to five polymorphs by varying the solution concentration.[10] Likewise, 1,3,5-tri(4-carboxyphenyl)benzene (**BTB**), a larger analogue of **TMA** which consists of a rigid additional phenyl spacer between central phenyl ring and each carboxylic group, displays three different concentration-dependent SAMNs.[12] Furthermore, the concentration effect has also been investigated for mixed SAMNs formed by **TMA** and **BTB**. Their relative concentration as well as overall solution concentration play a significant role.[14,22] In all these cases, the SAMNs formation follows the "concentration-in-control" self-assembly concept. However, such concentration effect has not been explored yet for the self-assembly of larger homologues of **TMA** such as 1,3,5-tris(4-carboxyphenylethynyl)-2,4,6-trimethylbenzene (**BT$_r$B**).[15] In these compounds, a phenylethynyl spacer connects the central phenyl ring and carboxylic acid groups.[23,24] In the case of **BT$_r$B**, the central phenyl ring is symmetrically substituted with three methyl groups. The rigid phenylethynyl spacer defines the position of the carboxylic acid groups, allowing in-plane hydrogen bonding interactions between carboxylic acid groups of adjacent molecules.[16] Moreover, an increased π-system promotes π–π stacking interactions between molecules in solution.[25] Indeed, such compounds having extended π-conjugation are known to form nanoscale molecular stacks in solution. However, their formation is solvent specific.[15]

UV-vis and scattering techniques have been widely used to investigate the formation of such aggregates in solution.[15,26,27] However, the effect of aggregation of solute molecules on self-assembly processes at the solution–solid interface, *i.e.* SAMN formation, has not been explored.[15] In particular, how the solution concentration influences the equilibrium between monomers and aggregates and its subsequent effect on the on-surface self-assembly behavior has yet to be investigated.

In this contribution, we demonstrate a counterintuitive inverse concentration dependent self-assembly behavior, as revealed by 1,3,5-tris(4-carboxyphenylethynyl)-2,4,6-trimethylbenzene (**BT$_r$B**) which can be considered a large analogue of 1,3,5-tris(4-carboxyphenyl)benzene (**BTB**). In contrast to **BTB**, **BT$_r$B** forms a low-density porous network at high solute concentrations and a high-density compact network at the same interface at lower solute concentrations. Fig. 1 schematically represents the inverse concentration dependence observed in the current work against that known previously for structurally similar **BTB** system. Here, we explore the origin of these contrasting concentration dependent self-assembly phenomena.

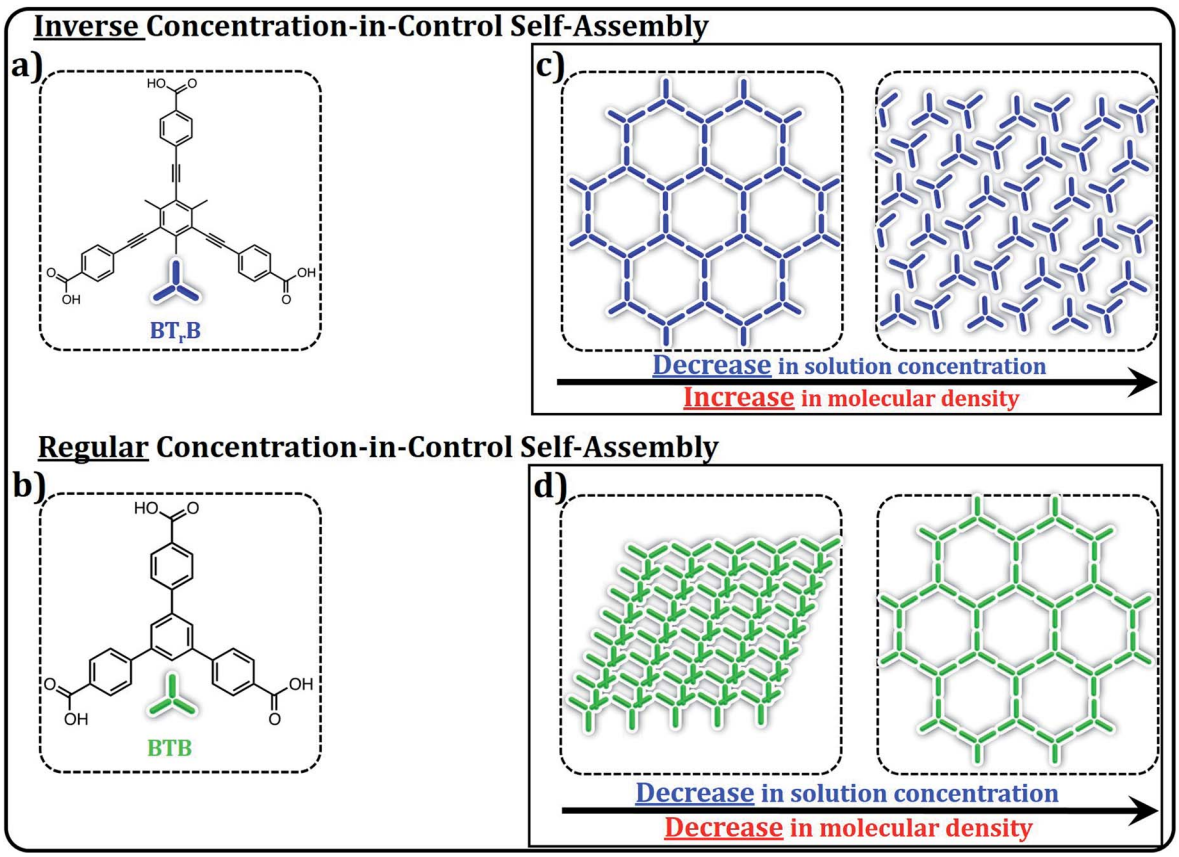

Fig. 1 A schematic summary of the main results presented in this work. (a) Molecular structure of BT$_r$B. (b) Molecular structure of BTB. (c) and (d) panels display the schematic illustration of the changes in the packing and packing density of the molecules as a function of solute concentration for BT$_r$B and BTB respectively. BTB shows the regular "concentration-in-control" trend, forming SAMNs of decreasing density upon decreasing solute concentration. BT$_r$B shows the unexpected opposite trend.

Results and discussion

As it is known that solute concentration plays a significant role on SAMN formation, it is in general good practice to investigate the impact of concentration for each compound in each solvent. This is also what we did upon investigating the self-assembly behavior of **BT$_r$B** at the interface between 1-heptanoic acid (HA) and HOPG. The bright-dark contrast in the STM images reflects the variations in distance of the STM tip with respect to the graphite substrate. For this kind of compounds and measuring conditions, the bright features correspond to the molecules as confirmed by their shape and size. **BT$_r$B** forms three different polymorphs depending on the concentration of the solution used. At the highest concentration ($C_{BTrB} = 4.2 \times 10^{-4}$ M to $C_{BTrB} = 2.2 \times 10^{-4}$ M) a low density, porous honeycomb phase of **BT$_r$B** was formed (**P-1**, Fig. 2a and d). In earlier work, this low-density phase has also been observed at nonanoic acid (NA)/HOPG interface for saturated solution.[15] The porous honeycomb phase is presumably, sustained *via* $R_2^2(8)$ hydrogen bonding between carboxylic groups. The unit cell consists of two **BT$_r$B** molecules and the packing density is 0.12 molecules per nm^2.

Surprisingly, at lower concentrations ($C_{BTrB} = 1.0 \times 10^{-4}$ M to $C_{BTrB} = 2.0 \times 10^{-5}$ M), **BT$_r$B** forms a relatively more compact network (**P-2**) (Fig. 2b and e). In contrast to the commonly observed head-to-head dimer units of carboxylic acids, the observed compact phase is probably sustained by a combination of typical intermolecular –O–H···O=C– hydrogen bonding interactions and relatively weak aromatic (Ar)–C–H···O=C– interactions between the **BT$_r$B** molecules. The unit cell contains also two **BT$_r$B** molecules but with a higher packing density (0.27 molecules per nm^2).

Upon diluting the solution further ($C_{BTrB} = 1.0 \times 10^{-5}$ M, to $C_{BTrB} = 6.7 \times 10^{-6}$ M) gives a "flower" type supramolecular network (**P-3**) (Fig. 2c and f). However, this flower type structure of **BT$_r$B** is different from the regular flower structure, for example, formed by trimesic acid.[28] Sixfold rings of **P-3** seem stabilized by atypical, relatively weak aromatic (Ar) –C–H···O= C– hydrogen bonding interactions between the **BT$_r$B** molecules. Each **BT$_r$B** molecule is interconnected with three adjacent

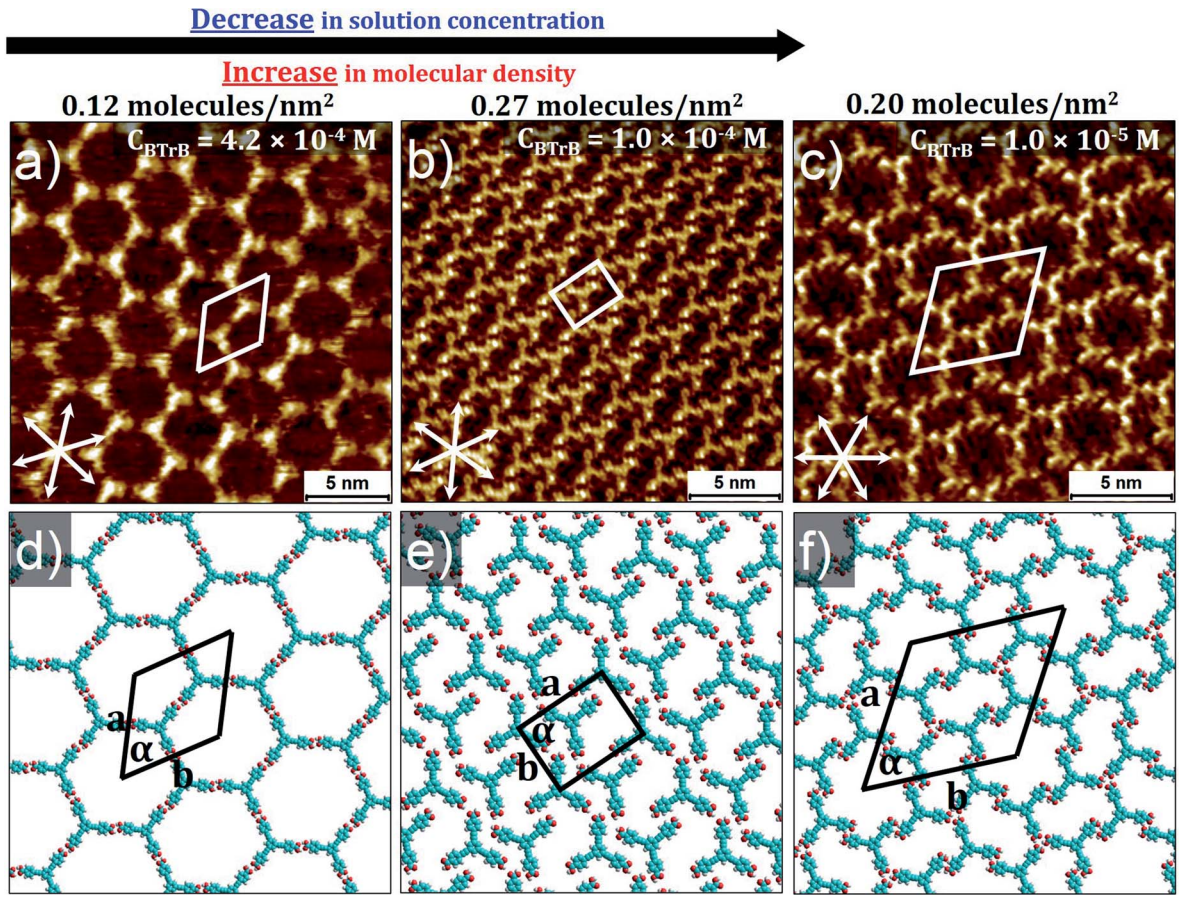

Fig. 2 Concentration dependent self-assembly behavior of **BT$_r$B** at HA/HOPG interface. Panel (a) shows low-density honeycomb porous network (**P-1**) at high solution concentration ($C_{BTrB} = 4.2 \times 10^{-4}$ M); corresponding molecular model with unit cell in panel (d). Panel (b) shows more compact porous network (**P-2**) at lower concentration ($C_{BTrB} = 1.0 \times 10^{-4}$ M); corresponding molecular model with unit cell in panel (e). Panel (c) shows flower type structure (**P-3**) of **BT$_r$B** at lowest solution concentration ($C_{BTrB} = 1.0 \times 10^{-5}$ M); corresponding molecular model with unit cell in panel (f). Graphite symmetry axes are indicated in lower left corner of STM images. Imaging parameters: (a) $I_{set} = 70$ pA, $V_{bias} = -1.1$ V; (b) $I_{set} = 100$ pA, $V_{bias} = -1.0$ V. (c) $I_{set} = 90$ pA, $V_{bias} = -1.0$ V. Unit cell parameters are provided in the Table 1. See ESI† for large-scale STM images.

Table 1 Structural parameters of the different monolayer phases obtained upon varying solution concentration[a]

BT_rB		Inverse concentration dependent self-assembly					BTB		Concentration dependent self-assembly				
		Unit cell parameters			ρ	N			Unit cell parameters			ρ	N
C	P	a (nm)	b (nm)	α (°)			C	P	a (nm)	b (nm)	α (°)		
4.2×10^{-4} M	**P-1**	4.1 ± 0.1	4.1 ± 0.1	60 ± 1	0.12	2	1.0×10^{-3} M	**P′-1**	3.3 ± 0.1	0.7 ± 0.1	82 ± 1	0.87	2
1.0×10^{-4} M	**P-2**	3.2 ± 0.1	2.3 ± 0.1	90 ± 1	0.27	2	1.0×10^{-4} M	**P′-2**	3.3 ± 0.1	1.8 ± 0.1	74 ± 1	0.34	2
1.0×10^{-5} M	**P-3**	5.5 ± 0.1	5.5 ± 0.1	60 ± 1	0.2	6	1.0×10^{-5} M	**P′-3**	3.2 ± 0.1	3.2 ± 0.1	60 ± 1	0.2	2
	P-4	2.0 ± 0.1	3.0 ± 0.1	81 ± 1	0.33	2	—	—	—	—	—	—	—

[a] ρ = density (molecules per nm^2), N = molecules per unit cell, C = concentration, P = polymorph.

molecules by these (Ar) –C–H···O=C– interactions. The unit cell comprises six BT_rB molecules and the packing density is now 0.20 molecules per nm^2, which is about 1.4 times lower than for **P-2** but still about 1.7 higher than **P-1**. Self-assembly behaviour of BT_rB has been previously studied by Gutzler *et al.* at NA/HOPG interface for saturated solution.[15] They could only observe honeycomb porous network (**P-1**) at the NA/HOPG interface. However, in the present contribution, we have used range of concentrations (4.2×10^{-4} M to 6.7×10^{-6} M) and found low-density honeycomb porous network (**P-1**) as well as other polymorphs such as low-density compact phase (**P-2**) and flower type structure (**P-3**) at heptanoic acid (HA)/HOPG

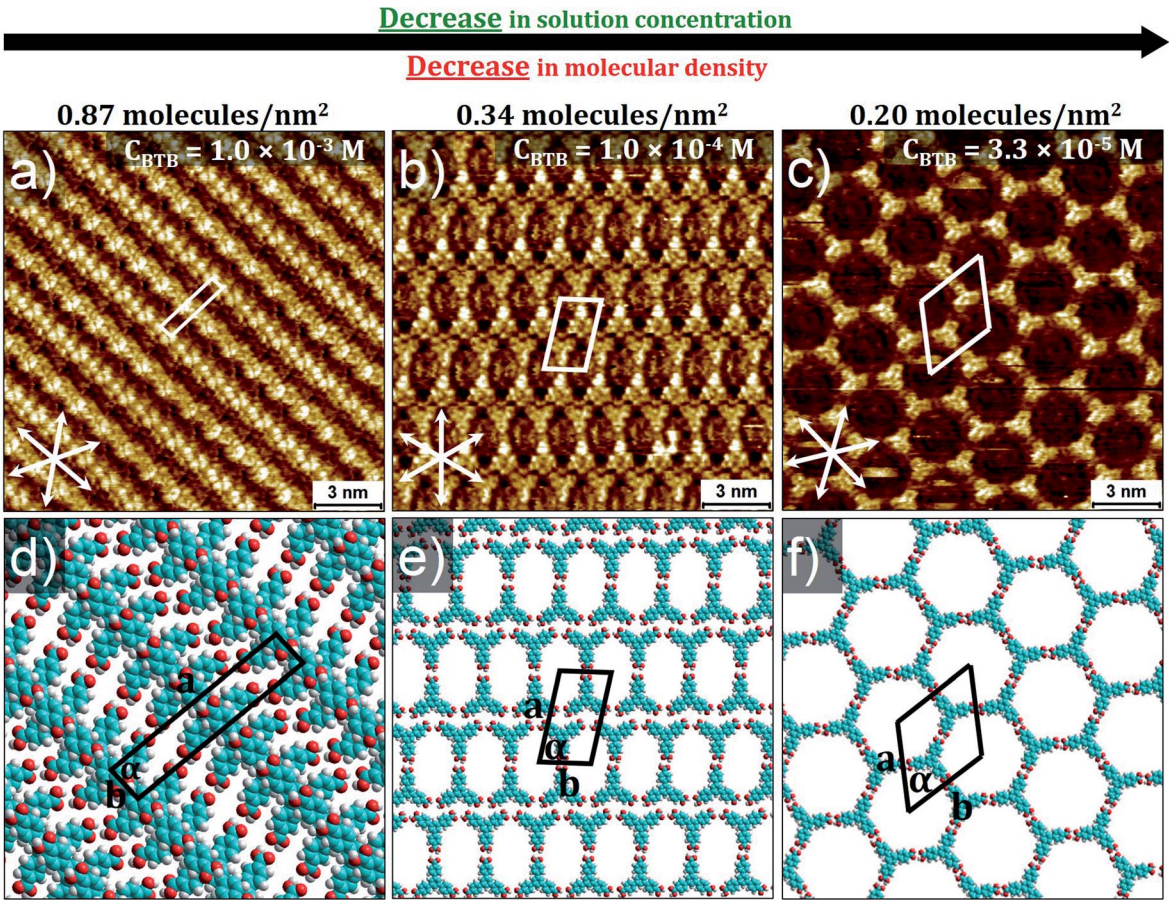

Fig. 3 Concentration dependent self-assembly behavior of **BTB** at HA/HOPG interface. Panel (a) shows high-density standing up row structure (**P′-1**) ($C_{BTB} = 1.0 \times 10^{-3}$ M); corresponding molecular model with unit cell in panel (d). Panel (b) shows lower-density oblique structure (**P′-2**) ($C_{BTB} = 1.0 \times 10^{-4}$ M); corresponding molecular model with unit cell in panel (e). Panel (c) shows low-density honeycomb porous network (**P′-3**) at low solution concentration ($C_{BTB} = 3.3 \times 10^{-5}$ M); corresponding molecular model with unit cell in panel (f). Graphite symmetry axes are indicated in lower left corner of STM images. Imaging parameters: (a) $I_{set} = 60$ pA, $V_{bias} = -1.2$ V; (b) $I_{set} = 100$ pA, $V_{bias} = -800$ mV; (c) $I_{set} = 90$ pA, $V_{bias} = -1.0$ V. Unit cell parameters are provided in Table 1. See the ESI† for large-scale STM images.

interface. The additional polymorphs attained in this investigation could be attributed to differences in the solution concentration.

It is imperative to mention here that the thin layer of solution may evaporate during the experiment and it could have a significant effect on the overall concentration of the solution. However, as mentioned above, the polymorphs **P-1**, **P-2** and **P-3** formed at room temperature are stable with-in the given concentration window. Therefore, the polymorph observed immediately after the deposition and several hours (8 hours) after deposition remained the same strongly indicating that the change in solution concentration due to evaporative loss of the solvent does not considerably affect the formation of a given polymorph.

To rationalize these intriguing results, we compared the results with **BTB**, a structurally related molecule. **BTB** displays rich self-assembly behavior at organic solution/HOPG interface. Depending on the type of solvents and range of concentrations, **BTB** gives three types of polymorphs such as standing up, oblique and honeycomb porous structures.[12,18,21] Fig. 3 shows the SAMN formation of **BTB** as a function of concentration. At high concentration (1×10^{-3} M), **BTB** forms densely packed rows (**P′-1**). The molecules are stacked face to face and are almost standing upright. The SAMN is sustained by intermolecular van der Waals and π–π interactions.[5] The unit cell contains two **BTB** molecules and the packing density is 0.87 molecules per nm^2.

At 1.0×10^{-4} M, **BTB** forms a lower-density porous supramolecular network (**P′-2**). The oblique structure is stabilized by a combination of most likely intermolecular –O–H···O=C– hydrogen bonding interactions and relatively weak aromatic –C–H···O=C– interactions between the **BTB** molecules. The unit cell contains two molecules and the packing density is 0.34 molecules per nm^2, about 2.5 times lower than that of **P′-1**.

Upon further decreasing the solution concentration ($C_{BTB} = 3.3 \times 10^{-5}$ M), a low-density porous honeycomb network is formed (**P′-3**). In this network, **BTB** building blocks self-assemble *via* $R_2^2(8)$ hydrogen bonding between carboxylic groups. The hexagonal unit cell contains two **BTB** molecules and the packing density is 0.20 molecules per nm^2. This systematic investigation indicates that **BTB** behaves in accordance with the conventional concentration dependent self-assembly.[12]

The question rises what is at the origin of the atypical concentration dependent behavior of **BT$_r$B**. Our hypothesis was that it relates more to what happens in solution than on the surface. In particular, formation of aggregates in solution would lower the effective concentration of **BT$_r$B** available to participate in SAMN formation. Therefore, we investigated the concentration dependency of the absorption spectra of **BT$_r$B** in heptanoic

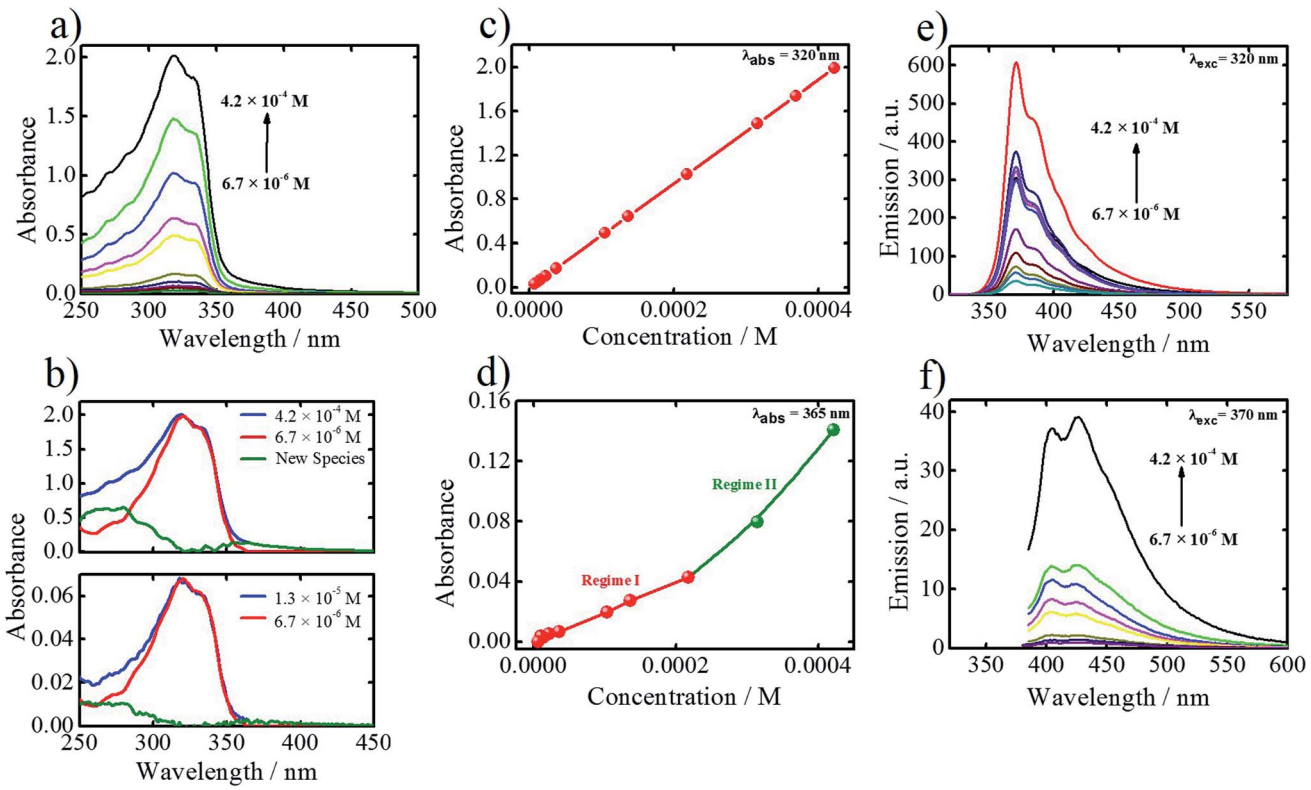

Fig. 4 Concentration dependent UV-vis spectroscopy and fluorescence spectroscopy of **BT$_r$B** in solution. (a) Absorption spectra of **BT$_r$B** at different solute concentrations. (b – top) Absorption spectra at the highest and lowest measured solute concentration, and difference spectrum. (b – bottom): same as for (b – top), but for a different high concentration of **BT$_r$B**. (c) Absorbance *versus* concentration at 320 nm. (d) Absorbance *versus* concentration at 365 nm. (e) Emission spectra of **BT$_r$B** at different solute concentrations ($\lambda_{exc} = 320$ nm). (f) Emission spectra of **BT$_r$B** at different solute concentrations ($\lambda_{exc} = 365$ nm).

acid (HA) *via* UV-vis spectroscopy. Upon increasing the concentration, the absorption at 320 nm follows the Lambert–Beer law (Fig. 4a and c) while at 365 nm, there is a deviation from the linear trend at higher concentrations (Fig. 4d). This is confirmed by subtracting the spectrum at high concentration from the spectrum obtained at the lowest concentration. The resultant spectrum shows a new band around 380 nm (Fig. 4b). Therefore, we tentatively assign the absorption at 365 nm to the presence of new species. Fig. 4e and f show emission spectra of **BT$_r$B** at excitation wavelengths 320 nm and 370 nm, respectively. The emission at 320 nm excitation mostly originates from the monomers, however, at high solution concentration, the emission spectrum broadens (FWHM = 2825 cm^{-1}) compared to the one obtained at the lowest concentration (FWHM = 2448 cm^{-1}) (Fig. S7 in ESI†). We attribute the origin of this broadening to the presence of a new emissive species. To confirm this assumption, emission spectra obtained upon exciting at 370 nm (where the monomer does not absorb) were recorded too (Fig. 4f). The results confirm that at low concentration, where the monomer is the main species, emission is negligible. Nevertheless, the emission intensity becomes more pronounced at higher concentrations, in line with the appearance of a new emissive species. To further prove the existence of these new species in the **BT$_r$B** solution, excitation spectra were also recorded. Fig. S8 (ESI†) shows a clear dependence between the excitation spectra and the concentration in the solution. While the 320 nm component is maximized at low concentrations, at higher ones, the 370 nm component is enhanced dramatically. The higher contribution of 370 nm at higher concentrated solutions induces a broadening in the excitation spectrum. Therefore, combination of absorption, emission and excitation spectra collectively prove the presence of new species at high solution concentrations. However, this behavior was not observed for a similar molecule, **BTB**, where no effect of the concentration on the features of absorption and emission spectra has been observed in the steady-state measurements (Fig. S9, ESI†).

Mechanism behind the inverse concentration dependent self-assembly

Based on the data analysis of the concentration dependent UV-vis data leading to the identification of a new species (Fig. 4), each UV-vis spectrum was subtracted from the monomeric spectrum (obtained at $C_{BTrB} = 6.7 \times 10^{-6}$ M), therefore the difference spectrum shown in Fig. 4b will have a strong contribution of the aggregated species. To get deeper insights about the concentration effect in the solution, we have plotted the integral intensity of monomers spectra and subtraction spectra *versus* the total concentration of the solution (Fig. S10†). At the first stage, as it should be expected, the monomer concentration is increasing upon increasing solution concentration. Although, the same occurs with the new species (aggregates), when the concentrations reach the 3.6×10^{-5} M, the new species (aggregates) contribution starts to increase faster by a factor of 2.5 (determined by the ratio of slopes). This observation is in agreement with normalized integral intensity as a function of concentration (Fig. S10b†), where the presence of new species (aggregates) is enhanced (0.1 to 0.28) upon increasing the solution concentration while the monomer contribution remains the same (0.7 to 0.76). Therefore, the presence of different polymorphs at the HA/HOPG interface might be related to concentration dependent monomer/aggregates contributions in solution. This explanation has been previously used for a similar molecule, where a pre-organization of the molecules in solution (monomer/aggregate) leads to a different assembly behavior at the liquid/solid interface and therefore polymorphism.[15,29]

To evaluate whether the effective monomer contribution is responsible for the observed inverse concentration dependent self-assembly of **BT$_r$B**, the phase density, which is defined as the number of molecules per square nanometer, has been plotted as a function of concentration. Fig. 5a shows plots of **BT$_r$B** phase density *versus* concentration. The figure shows that at the highest solution concentration regime ($C_{BTrB} = 4.2 \times 10^{-4}$ M to $C_{BTrB} = 2.2 \times 10^{-4}$ M), **BT$_r$B** forms a low-density honeycomb porous network (**P-1**; the phase density is 0.12 molecules per nm^2).

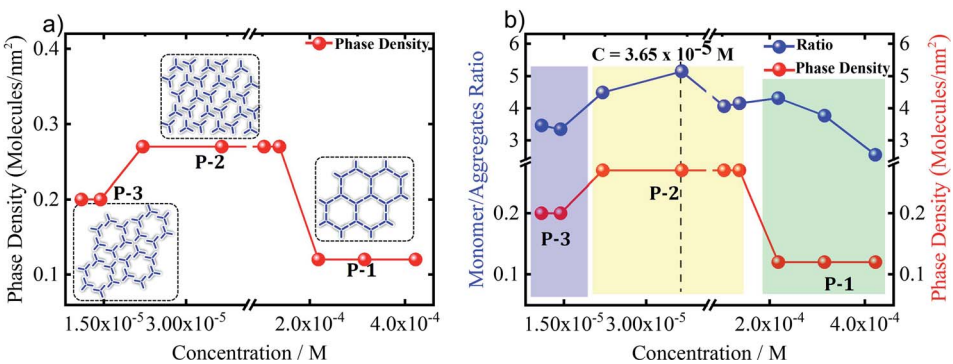

Fig. 5 (a) Plots of molecular phase density of **BT$_r$B** as a function of concentration. (b) Monomer/aggregate ratio and plots of molecular phase density of **BT$_r$B** as a function of concentration.

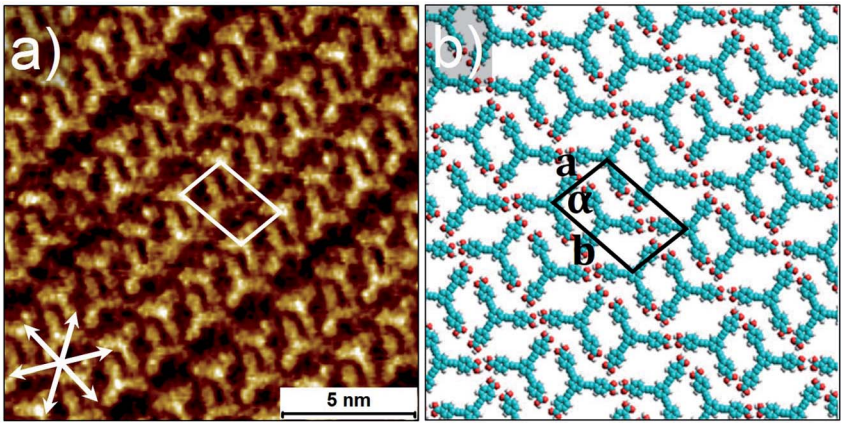

Fig. 6 STM image acquired after annealing the sample. Panel (a) shows highest density compact network (P-4) at the range of solution concentrations ($C_{BTrB} = 4.2 \times 10^{-4}$ M to $C_{BTrB} = 1.0 \times 10^{-5}$ M); corresponding molecular model with unit cell in panel (b). Graphite symmetry axes are indicated in lower left corner of STM image. Imaging parameters: (a) $I_{set} = 80$ pA, $V_{bias} = -1.0$ V. Unit cell parameters are provided in the Table 1. See ESI† for large-scale STM images.

However, upon lowering the concentration (at $C_{BTrB} = 1.0 \times 10^{-4}$ M to $C_{BTrB} = 2.0 \times 10^{-5}$ M range), **BT$_r$B** gives a low-density compact phase (**P-2**; the phase density of 0.27 molecules per nm^2). The increase in the phase density of **BT$_r$B** is in good agreement with the monomer/aggregate ratio, as it also shows some increase upon lowering the solute concentration (Fig. 5b). A further decrease in concentration (at $C_{BTrB} = 1.0 \times 10^{-5}$ M to $C_{BTrB} = 6.7 \times 10^{-6}$ M range), leads to the formation of a new phase, the displaced flower type structure (**P-3**; the phase density of 0.20 molecules per nm^2). Comparing Fig. 5a and b indicates that the phase density and monomer/aggregate ratio follow the same trend. This suggests that the atypical concentration dependent self-assembly behavior of **BT$_r$B** is related to the free monomer concentration. Comparing **P-2** and **P-1**, **P-2**, the low-density compact phase, is formed at the highest monomer-to-aggregate ratio in solution, *i.e.* highest monomer contribution. However, the fact that the phase of intermediate density (**P-3**) is observed at the lowest solution concentrations investigated indicates that additional factors should be taken into account to explain the atypical concentration-in-control self-assembly behavior. Note that **P-4**, a new polymorph, is formed upon annealing the sample for 5 minutes at 80 °C, followed by imaging at room temperature (RT), regardless of the concentration (Fig. 6a and b). This phase is probably sustained by a combination of typical intermolecular –O–H···O═C– hydrogen bonding interactions and relatively weak aromatic (Ar)–C–H···O═C– interactions between the **BT$_r$B** molecules. The unit cell contains two **BT$_r$B** molecules but with a higher packing density (0.33 molecules per nm^2). The higher packing density upon annealing is probably partly due to the higher monomer to aggregate ratio and increased monomer concentration in the solution at high temperature. This is confirmed by comparing the concentration dependent emission spectra at 25 °C and 80 °C (Fig. S12†). Perhaps more important is the observation that the formation of **P-4** phase occurs upon annealing. This may suggest that **P-4** is the thermodynamic phase, at the annealing temperature, and potentially also at room temperature and that the formation of the other three phases (**P-1**, **P-2**, and **P-3**) is, at least in part, kinetically favored. This remains speculative though, as the annealing process leading to the formation of **P-4** may lead to significant solvent evaporation, and therefore also a strong change in concentration.

As we cannot monitor this directly, we are somehow left to speculate. We propose that at the highest concentration, the aggregates start to dominate the solution composition and might "screen" the monomers from interacting with the surface, by blocking the surface, resulting in a low effective monomer concentration, *i.e.* lower than what should be expected based on the solution composition, and potentially also a lower adsorption rate. This could lead to the formation of the lowest density polymorph (**P-1**). Upon decreasing the concentration, the monomer/aggregate ratio increases, as well as potentially the adsorption rate favoring the formation of a more compact porous network (**P-2**). Upon diluting the solution further ($<C_{BTrB} = 3.6 \times 10^{-5}$ M) the monomer/aggregate ratio still increases, but the effective monomer concentration now decreases (Fig. 6). It is imperative to mention here that the low effective monomer concentrations at the lowest and highest concentration are different. The low effective monomer concentration at the highest concentration probed is due to the high aggregate/monomer ratio combined with a potential screening effect, whereas at the lowest concentration, it reflects the low solute concentration. Therefore, upon lowering the concentration, the low effective monomer concentration gives rise to the low-density displaced flower type network (**P-3**), the expected outcome of a regular concentration-in-control trend.

Conclusions and outlook

So far, the "concentration-in-control" concept has governed the self-assembly behavior of numerous organic compounds at solution–solid interfaces. According to this concept, which assumes thermodynamic equilibrium, molecules form high- and low-density supramolecular networks at high and low

solution concentrations, respectively. In contrast to this, here we have demonstrated, for the first time, the formation of a low-density porous network at higher solution concentrations and higher-density more compact porous network at lower solute concentrations. The "break down" of this "concentration-in-control" self-assembly concept has been explained using combined principles of supramolecular chemistry in solution and on surfaces, surface science and solution chemistry. In particular, the concentration dependent aggregation plays a key role in this intriguing behavior. The delicate balance between the monomers and preformed aggregates in the solution, in combination with kinetic effects, drives the inverse concentration dependent self-assembly at the solution–solid interface.

This study shows once more the important role that solution composition plays on self-assembly phenomena at liquid–solid interfaces. While in other studies the adsorption of aggregate species has led to high-density supramolecular structures irrespective of concentration,[15] here we are facing the impact of aggregation in solution has a significant influence on the effective monomer concentration, and the interplay between thermodynamics and kinetics. This interplay might be complex, and it will remain hard to predict the outcome of an interfacial self-assembly process. It is once more a wake-up call of the importance to systemically probe concentration and temperature dependent effects on the self-assembly at liquid–solid interfaces in general, and the formation of self-assembled molecular networks in particular. However, its impact goes beyond SAMNs. Adsorption at liquid–solid interface is a complex process, in particular in case of aggregation phenomena in solution, which may be static or dynamic on the time scale of adsorption and self-assembly processes on the solid substrate. Therefore, the widely accepted protocol of drop casting, in many cases followed by solvent evaporation, and characterization of the on-surface "deposits", to gain information on the solution composition, should be done with great care.

Experimental methods

Scanning tunneling microscopy (STM)

1,3,5-Tris(4-carboxyphenylethynyl)-2,4,6-trimethylbenzene (**BT$_r$B**) was synthesized according to reported methods.,[15,24] 1,3,5-tris(4-carboxyphenyl)benzene (**BTB**) was purchased from Aldrich and the stated purity is 98+%. Stock solutions of **BT$_r$B** ($C_{BTrB} = 1.0 \times 10^{-3}$ M) and **BTB** ($C_{BTB} = 1.0 \times 10^{-3}$ M) were prepared by dissolving the appropriate amount of solid in 1-heptanoic acid (HA) (Sigma-Aldrich ≥ 99%). The stock solutions were diluted further with HA to make a concentration series. All STM experiments were performed at room temperature (21–23 °C) using a PicoLE (Agilent) machine operating in constant-current mode with the tip immersed in the supernatant liquid. STM tips were prepared by mechanically cutting a Pt/Ir wire (80%/20%, diameter 0.2 mm). Prior to imaging, a drop of solution was placed onto a freshly cleaved surface of highly oriented pyrolytic graphite (HOPG, grade ZYB, Advanced Ceramics Inc., Cleveland, USA). The experiments were repeated in 2–3 sessions using different tips to check for reproducibility and to avoid experimental artefacts, if any. For analysis purposes, recording of a monolayer image was followed by imaging the graphite substrate underneath under the same experimental conditions, except for increasing the current and lowering the bias. The images were corrected for drift *via* Scanning Probe Image Processor (SPIP) software (Image Metrology ApS), using the recorded graphite images for calibration purposes, allowing a more accurate unit cell determination. The unit cell parameters were determined by examining at least 4 images and only the average values are reported. The images are Gaussian filtered. The imaging parameters are indicated in the figure caption: tunneling current (I_{set}), and sample bias (V_{bias}). The molecular models were built using Hyperchem™ 7.0 program.

UV-vis spectroscopy

All stationary measurements have been recorded using a spectrophotometer (Lambda-950 spectrometer) and a FLS920 spectrofluorometer (Edinburgh Instrument Ltd, Livingston, UK). The spectrometers were corrected for the wavelength dependence of the throughput of the emission monochromator and the sensitivity of the detector. The optical density at the absorption maximum of all solutions was kept below 0.1 in a 1 cm cuvette (10^{-5} M). The EQE was measured using an integrating sphere (Labsphere) coupled to the abovementioned fluorimeter through optical fibers. Barium sulfate was used during the EQE measurement as fully scattering reference.

Data availability

Large-scale STM images of **BT$_r$B** and **BTB**, emission spectra of **BT$_r$B** at low and high solution concentrations, concentration dependent excitation spectra of **BT$_r$B**, concentration dependent absorption and emission spectra of **BTB**, integral intensity and normalized integral intensity of **BT$_r$B** monomers and aggregates as a function of concentration, large-scale STM image of **BT$_r$B** highest density compact network and the temperature dependent emission spectra of the **BT$_r$B** at different excitation wavelengths are provided in the ESI.†

Author contributions

GM. V., C. M., K. M. and SDF designed the research; B. D. and G. H. synthesized the compounds; GM. V. and C. M. performed the experiments and analyzed the data; all the authors contributed to the results and discussion. All the authors contributed to writing the manuscript.

Conflicts of interest

The authors declare no competing financial interest.

Acknowledgements

The authors gratefully acknowledge financial support from the Fund of Scientific Research Flanders (FWO), KU Leuven – Internal Funds (C14/19/079). This work was in part supported by FWO under EOS 30489208. GM. V. acknowledges the FWO

fellowship award (No. 1269221N). C. M. thanks the FWO for the fellowships received (12J1719N and 12J1716N). G. H. thanks the MIC, Spain (project pid2019-104125RB-100) for financial support.

References

1 J. A. Theobald, N. S. Oxtoby, M. A. Phillips, N. R. Champness and P. H. Beton, Controlling Molecular Deposition and Layer Structure with Supramolecular Surface Assemblies, *Nature*, 2003, **424**, 1029.

2 S. Lei, K. Tahara, F. C. De Schryver, M. Van der Auweraer, Y. Tobe and S. De Feyter, One Building Block, Two Different Supramolecular Surface-Confined Patterns: Concentration in Control at the Solid–Liquid Interface, *Angew. Chem., Int. Ed.*, 2008, **47**, 2964–2968.

3 K. S. Mali, J. Adisoejoso, E. Ghijsens, I. De Cat and S. De Feyter, Exploring the Complexity of Supramolecular Interactions for Patterning at the Liquid–Solid Interface, *Acc. Chem. Res.*, 2012, **45**, 1309–1320.

4 T. Kudernac, S. Lei, J. A. A. W. Elemans and S. De Feyter, Two-dimensional supramolecular self-assembly: nanoporous networks on surfaces, *Chem. Soc. Rev.*, 2009, **38**, 402–421.

5 R. Gutzler, T. Sirtl, J. F. Dienstmaier, K. Mahata, W. M. Heckl, M. Schmittel and M. Lackinger, Reversible Phase Transitions in Self-Assembled Monolayers at the Liquid−Solid Interface: Temperature-Controlled Opening and Closing of Nanopores, *J. Am. Chem. Soc.*, 2010, **132**, 5084–5090.

6 G. M. Florio, K. A. Stiso and J. S. Campanelli, Surface Patterning of Benzenecarboxylic Acids: Influence of Structure, Solvent, and Concentration on Molecular Self-Assembly, *J. Phys. Chem. C*, 2012, **116**, 18160–18174.

7 K.-W. Park, J. Adisoejoso, J. Plas, J. Hong, K. Müllen and S. De Feyter, Self-Assembly Behavior of Alkylated Isophthalic Acids Revisited: Concentration in Control and Guest-Induced Phase Transformation, *Langmuir*, 2014, **30**, 15206–15211.

8 X. Shen, X. Wei, P. Tan, Y. Yu, B. Yang, Z. Gong, H. Zhang, H. Lin, Y. Li, Q. Li, Y. Xie and L. Chi, Concentration-Controlled Reversible Phase Transitions in Self-Assembled Monolayers on HOPG Surfaces, *Small*, 2015, **11**, 2284–2290.

9 A. Ciesielski, P. J. Szabelski, W. Rżysko, A. Cadeddu, T. R. Cook, P. J. Stang and P. Samorì, Concentration-Dependent Supramolecular Engineering of Hydrogen-Bonded Nanostructures at Surfaces: Predicting Self-Assembly in 2D, *J. Am. Chem. Soc.*, 2013, **135**, 6942–6950.

10 N. Thi Ngoc Ha, T. G. Gopakumar and M. Hietschold, Polymorphism Driven by Concentration at the Solid–Liquid Interface, *J. Phys. Chem. C*, 2011, **115**, 21743–21749.

11 M. O. Blunt, J. Adisoejoso, K. Tahara, K. Katayama, M. Van der Auweraer, Y. Tobe and S. De Feyter, Temperature-Induced Structural Phase Transitions in a Two-Dimensional Self-Assembled Network, *J. Am. Chem. Soc.*, 2013, **135**, 12068–12075.

12 F. P. Cometto, K. Kern and M. Lingenfelder, Local Conformational Switching of Supramolecular Networks at the Solid/Liquid Interface, *ACS Nano*, 2015, **9**, 5544–5550.

13 M. Lackinger, S. Griessl, W. M. Heckl, M. Hietschold and G. W. Flynn, Self-Assembly of Trimesic Acid at the Liquid−Solid Interface Study of Solvent-Induced Polymorphism, *Langmuir*, 2005, **21**, 4984–4988.

14 L. Kampschulte, T. L. Werblowsky, R. S. K. Kishore, M. Schmittel, W. M. Heckl and M. Lackinger, Thermodynamical Equilibrium of Binary Supramolecular Networks at the Liquid−Solid Interface, *J. Am. Chem. Soc.*, 2008, **130**, 8502–8507.

15 R. Gutzler, S. Lappe, K. Mahata, M. Schmittel, W. M. Heckl and M. Lackinger, Aromatic interaction vs.hydrogen bonding in self-assembly at the liquid–solid interface, *Chem. Commun.*, 2009, 680–682.

16 M. Lackinger and W. M. Heckl, Carboxylic Acids: Versatile Building Blocks and Mediators for Two-Dimensional Supramolecular Self-Assembly, *Langmuir*, 2009, **25**, 11307–11321.

17 J. Teyssandier, S. D. Feyter and K. S. Mali, Host–guest chemistry in two-dimensional supramolecular networks, *Chem. Commun.*, 2016, **52**, 11465–11487.

18 L. Kampschulte, M. Lackinger, A.-K. Maier, R. S. K. Kishore, S. Griessl, M. Schmittel and W. M. Heckl, Solvent Induced Polymorphism in Supramolecular 1,3,5-Benzenetribenzoic Acid Monolayers, *J. Phys. Chem. B*, 2006, **110**, 10829–10836.

19 F. Silly, Two-Dimensional 1,3,5-Tris(4-carboxyphenyl) benzene Self-Assembly at the 1-Phenyloctane/Graphite Interface Revisited, *J. Phys. Chem. C*, 2012, **116**, 10029–10032.

20 M. Ruben, D. Payer, A. Landa, A. Comisso, C. Gattinoni, N. Lin, J.-P. Collin, J.-P. Sauvage, A. De Vita and K. Kern, 2D Supramolecular Assemblies of Benzene-1,3,5-triyl-tribenzoic Acid: Temperature-Induced Phase Transformations and Hierarchical Organization with Macrocyclic Molecules, *J. Am. Chem. Soc.*, 2006, **128**, 15644–15651.

21 S.-L. Lee, Y. Fang, G. Velpula, F. P. Cometto, M. Lingenfelder, K. Müllen, K. S. Mali and S. De Feyter, Reversible Local and Global Switching in Multicomponent Supramolecular Networks: Controlled Guest Release and Capture at the Solution/Solid Interface, *ACS Nano*, 2015, **9**, 11608–11617.

22 G. Velpula, J. Teyssandier, S. De Feyter and K. S. Mali, Nanoscale Control over the Mixing Behavior of Surface-Confined Bicomponent Supramolecular Networks Using an Oriented External Electric Field, *ACS Nano*, 2017, **11**, 10903–10913.

23 R. K. Castellano and J. Rebek, Formation of Discrete, Functional Assemblies and Informational Polymers through the Hydrogen-Bonding Preferences of Calixarene Aryl and Sulfonyl Tetraureas, *J. Am. Chem. Soc.*, 1998, **120**, 3657–3663.

24 G. Hennrich, I. Asselberghs, K. Clays and A. Persoons, Tuning Octopolar NLO Chromophores: Synthesis and Spectroscopic Characterization of Persubstituted 1,3,5-Tris(ethynylphenyl)benzenes, *J. Org. Chem.*, 2004, **69**, 5077–5081.

25 G. Hennrich, B. Nieto-Ortega, B. Gómez-Lor, E. Gutierrez, L. de Vega, E. Cavero, F. J. Ramírez, J. T. López Navarrete and J. Casado, Controlling the Macroscopic Chirality of Organic Materials Based on 1,3,5-Trialkynylbenzenes, *Eur. J. Org. Chem.*, 2012, **2012**, 1577–1582.

26 T. Seki, S. Yagai, T. Karatsu and A. Kitamura, Formation of Supramolecular Polymers and Discrete Dimers of Perylene Bisimide Dyes Based on Melamine–Cyanurates Hydrogen-Bonding Interactions, *J. Org. Chem.*, 2008, **73**, 3328–3335.

27 F. Würthner, S. Yao, T. Debaerdemaeker and R. Wortmann, Dimerization of Merocyanine Dyes. Structural and Energetic Characterization of Dipolar Dye Aggregates and Implications for Nonlinear Optical Materials, *J. Am. Chem. Soc.*, 2002, **124**, 9431–9447.

28 S. Griessl, M. Lackinger, M. Edelwirth, M. Hietschold and W. M. Heckl, Self-Assembled Two-Dimensional Molecular Host-Guest Architectures From Trimesic Acid, *Single Molecules*, 2002, **3**, 25–31.

29 T. Kudernac, A. K. Mandal and J. Huskens, Bicomponent H-Bonded Porous Molecular Networks at the Liquid–Solid Interface: What Is the Influence of Preorganization in Solution?, *Langmuir*, 2015, **31**, 157–163.